Journal of Alloys and Compounds 568 (2013) 106–111

Contents lists available at SciVerse ScienceDirect

Journal of Alloys and Compounds

journal homepage: www.elsevier.com/locate/jalcom

Solid-state reactions during mechanical milling of Fe–Al under nitrogen atmosphere

Y. Jiraskova [a,*], J. Bursik [a], J. Cizek [b], D. Jancik [c]

[a] Institute of Physics of Materials, AS CR, Žižkova 22, CZ-616 62 Brno, Czech Republic
[b] Charles University in Prague, Faculty of Mathematics and Physics, Department of Low Temperature Physics, V Holesovickach 2, CZ-18000 Praha 8, Czech Republic
[c] Palacky University in Olomouc, Faculty of Science, Centre for Nanomaterial Research, Slechtitelu 11, CZ-783 71 Olomouc, Czech Republic

ARTICLE INFO

Article history:
Received 14 December 2012
Received in revised form 13 February 2013
Accepted 3 March 2013
Available online 25 March 2013

Keywords:
Milling
Mechanical alloying
Mössbauer phase analysis
Fe–Al alloy
Microstructure

ABSTRACT

The sequence of solid-state reactions of iron and aluminum powders of approximate composition 82:18 in nitrogen atmosphere is followed during high energy ball milling. As an alternative, pieces prepared from $Fe_{82}Al_{18}$ ingot as the starting product are exposed to milling under nitrogen as well. X-ray diffraction, Mössbauer spectrometry, and electron microscopy supported by magnetic measurements have been applied to follow changes in the microstructure, phase composition and magnetic properties in dependence on milling time.

The electron microscope observations show morphology of powder particles and changes in chemical composition during mechanical treatment. The changes in composition are observed at samples formed by mechanical alloying. On the other hand the composition of $Fe_{82}Al_{18}$ pieces is influenced by milling only weakly. The analysis of the room temperature X-ray diffraction patterns and of the Mössbauer spectra reflects an alloying process of elemental Fe and Al powders already after 5 h of milling and a stepwise pulverization of the initial $Fe_{82}Al_{18}$ bulk alloy. This leads in both cases to formation of a micro(nano)crystalline material in a metastable state with large amount of defects, and microstructure influencing its physical properties documented by magnetic measurements. Moreover the nitrogen atmosphere leads to formation of ferromagnetic nitride in a process of mechanical alloying while the milled $Fe_{82}Al_{18}$ is almost insensitive to the nitrogen atmosphere.

1. Introduction

FeAl based alloys are often exploited materials for their reasonable low cost, low density, high temperature corrosion resistance, and good intermediate-temperature mechanical properties [1–3]. Their constituents are mutually completely soluble [4] and some of these systems display unique magnetic properties. In the Fe-rich region the Fe–Al yields a disordered body-centered-cubic (bcc) structure up to 22 at.% Al at room temperature. Moreover a variety of intermetallic phases such as, e.g. Fe_3Al, FeAl, $Fe_{13}Al$, are formed in this system. The first mentioned, Fe_3Al, has $D0_3$ cubic structure and exists over the concentration range 18–37 at.%Al. The Fe–Al alloys ith Al content between 37 and 50 at.% are ordered in a stable B2 structure. The room temperature magnetic moment of ordered Fe–Al alloys decreases with increasing Al content up to 20 at.% slowly while faster decrease is observed for higher Al concentrations. At 30 at.% Al, the average magnetic moment per Fe atom steeply decreases from approx. 2.0 to 0.7 μ_B and all alloys above this Al concentration are paramagnetic at room temperature [5]. On the other hand the disordered Fe–Al alloys are ferromagnetic also for concentrations of aluminum above 35 at.% [6,7]. It is well-known that materials of the same nominal composition but processed in a different way, e.g., classical melting and casting, mechanical alloying, thermo-mechanical treatment etc., often yield different microstructure, different final composition and defects that are connected with different physical properties. This fact was a motivation also for present investigations of the Fe–Al system with Al content of 18 at.%. This composition is at the boundary between the highly disordered bcc Fe–Al solid solution of A2 structure and the $D0_3$ structure [4]. The first material was prepared by mechanical alloying (MA) from the initial Fe and Al powders, the second one by mechanical milling (MM) of the pre-alloyed pieces of the same nominal composition. Both procedures were realized by high-energy ball milling. Mechanical alloying and milling are well-established methods of production of various materials, as nanocrystalline alloys, amorphous compounds, quasi-crystals, etc. [8,9]. During MA and MM a heavy deformation is introduced into the milled material. This is manifested by the presence of crystal defects such as dislocations, vacancies, stacking faults, and an increased number of grain boundaries. The formation of defect structure initially enhances the mutual diffusivity of

* Corresponding author. Tel.: +420 532290446; fax: +420 541218657.
E-mail address: jirasko@ipm.cz (Y. Jiraskova).

0925-8388/$ - see front matter © 2013 Elsevier B.V. All rights reserved.
http://dx.doi.org/10.1016/j.jallcom.2013.03.087

elements but simultaneously the microstructure refinement decreases the diffusion distances. Additionally, the diffusion behavior can be influenced by temperature increase during milling process and the milling atmosphere can either inhibit contamination of the powders and their oxidation or contribute to formation of other phases as, e.g., nitrides. It is clear that both MA and MM are complicated processes evoking many problems to be solved.

2. Experimental

For the mechanical milling, high purity Fe (99.99%) and Al (99.99%) input rods were arc melted in Ar atmosphere gettered by Ti. From an ingot of nominal composition $Fe_{82}Al_{18}$ small pieces were cut and consequently step-wise milled. After t = 10, 20, and 30 h of milling steps the pulverized material was taken away and samples (denoted MM/t) for further experimental investigations prepared. For the mechanical alloying, the Fe (10 μm) and Al (40 μm) powders corresponding to $Fe_{82}Al_{18}$ composition were placed into a stainless steel vial and initially mixed in the rotating vial without balls by 200 rpm for 2 min. The milling was performed step-wise and after 5, 10, 20, and 30 h of milling the powder was taken away. These samples are denoted MA/t. For both experiments stainless steel balls, each of 5 mm in diameter, were added to the Fe–Al mixture preserving ball-to-powder weight ratio 10:1. The milling was done using a Fritsch planetary ball mill Pulverisette 7 premium line under nitrogen atmosphere. The speed of rotation was 450 rpm. To avoid sample heating the regime was chosen in such a way that 60 min of milling were followed by 60 min of pause (1 cycle). Powder samples were removed at specific times for the elemental and microstructural analysis.

A TESCAN LYRA 3XMU FEG/SEM scanning electron microscope (SEM) working at accelerating voltage of 15 kV was used to follow the surface morphology and microstructure. Samples for SEM were prepared by spreading a small amount of powder on a sticky conductive tape.

An X'PERT – PRO diffractometer with Co Kα radiation (λ = 0.17902 nm) was used to study the structural changes occurring in the mixture in various stages during milling. Small amount of powder was spread in a uniform compact layer on a Si plate. The measurements were done from 20° to 135° in steps of 0.008°, with time 6 s/step at room temperature (RT). Detailed analysis of powder patterns was realized using the Rietveld structure refinement method [10] and the ICSD database of inorganic and related structures.

Mössbauer spectrometry was used to gain insight into the structural evolution of the local environment of the iron atoms. The measurements were carried out at room temperature in standard transmission geometry using a ^{57}Co(Rh) source. The calibration of velocity scale was performed with α-Fe and isomer shifts are given with respect to the RT Mössbauer spectrum of α-Fe. All spectra were evaluated within the transmission integral approach using the program CONFIT [11]. In the measured Mössbauer spectrum the crystalline components are represented by discrete single-, double-, and/or six-line Lorentzian sub-spectra determined by discrete values of hyperfine parameters: isomer shift(s), quadrupole splitting(s) and hyperfine induction(s), corresponding to paramagnetic and/or ferromagnetic phases, respectively. The interfacial phase is represented by a distribution of hyperfine parameters (quadrupole and/or magnetic splitting) in a form of Gaussian distribution. All components are further described by their intensities.

Hysteresis loops in the external field of ±796 kA/m and thermomagnetic curves in the external magnetic field of 4 kA/m and temperature increase of 4 K/min in vacuum were obtained using a vibrating sample magnetometer. These parameters were kept the same for all measurements.

3. Results and discussion

3.1. Electron microscopy

Four MA samples and three MM samples were studied using SEM. The structure of samples MA/5 and MA/30 is shown in Fig. 1. In the whole MA series, agglomerates of the large (up to 100 μm) and small (around 1 μm or even submicron) grains are visible. Without substantial change in the grain size, the chemical composition of the grains changes with the time of milling. At least 30 objects were analyzed in each sample. The averaged results of EDX analyses do not reveal significant differences. However, the details of composition changes during ball milling are well visible on histograms in Fig. 2. Distribution of Fe content in the sample MA/5 (Fig. 2a) shows a certain amount of Fe-rich grains (peak maximum at 96 at.% Fe) and another broad peak situated around 79 at.% Fe. After longer milling time the sample MA/30 gives a histogram (Fig. 2b) with two peaks shifted towards lower Fe concentrations (one peak around 68%, the other one around 84 at.% Fe). This peak separation might be related to a formation of two phases – the ordered Fe_3Al phase and the terminal solid solution.

The features of MM samples after 10 (a) and 30 (b) h of milling are depicted in Fig. 3. In contrast to the MA series, the MM series reveals only very small changes in chemical composition, but pronounced changes in grain size with milling time. The coarse grains (20–100 μm) in the sample MM/10 (Fig. 3a) scale subsequently down to about 0.5–10 μm in the sample MM/30 (Fig. 3b), which is the finest powder size of all samples reported in this work.

3.2. X-ray diffraction

X-ray diffraction measurements were used to follow changes in the composition and crystallite size of both types of samples. Differences between MA and MM samples after 10 and 30 h of mechanical treatment are seen in diffraction patterns in Fig. 4 (upper panel). The patterns of MA/10 and MA/30 samples are characterized by dominating peaks of a bcc structure of α–Fe denoted by "△" whereas the diffraction lines broaden asymmetrically in direction of lower angles. It reflects a distribution of lattice parameters in the forming alloyed phase mixtures. The results obtained by analyzing of diffraction data using the Rietveld structure refinement method are summarized in Table 1. It is seen that already after 5 h of milling the α–Fe phase coexists with the bcc-$Fe_{1-x}Al_x$. This is in good agreement with other studies, e.g. [12], despite the fact that the results often depend on the milling conditions and initial input powder mixture. In the present study the line broadening, in detail well visible in the bottom panel of Fig. 4, is caused by the other coexisting phases namely ε-Fe_xN and Fe_2Al_5. The physical parameters slightly change in dependence on the milling time as seen in Table 1. The lattice parameter 0.2904 nm of the forming bcc Fe–Al phase achieved after 5 h of milling is nearly independent on milling time as long as it decreases to 0.2898 nm after 30 h of milling. A very similar result was obtained for an Fe alloy with 20 at.%Al, e.g. in Ref. [13]. The parameter 0.2898 nm is comparable with that one obtained for the bulk $Fe_{82}Al_{18}$ alloy the composition of which was checked by EDX and it was 17.7 ± 0.7 at.% Al. The nitrogen concentration, x, in the ε-Fe_xN was reported to have a relation with the lattice parameters a, c (in nm) of the hcp structure as follows [14]:

$$x_a = 0.0673/(a - 0.44709) \text{ and } x_c = 0.0318/(c - 0.42723),$$

where x_a and x_c should equal each other for stress-free samples. In the present case the calculations of x in the ε-Fe_xN using experimentally obtained lattice parameters (a, c) have brought the best result for the MA/20 sample, namely x_a = 2.6 and x_c = 2.7. At other samples the relative difference of x_a and x_c was between 20% and 50% that can be ascribed to the unequal high plastic deformation and induced stress relief. The formation of the Fe_2Al_5 phase was probably first observed by Cardellini et al. [15] and recently by Yelsukov et al. [16]. Cardellini et al. observed the formation of a non-magnetic component after 2 h of milling of the Fe-25 at.%Al mixture and indentified this component as Fe_2Al_5 after temperature treatment at 430 °C. On the other hand, Yelsukov et al. studied solid state reactions by ball milling of the Fe–Al mixture with Al content in the opposite side of phase diagram, Fe-68 at.% Al, and detected the Fe_2Al_5 after 2.5 h of milling followed by annealing at 500 °C. The content of the Fe_2Al_5 in the present study has changed between 16% and 20% whereas the content of bcc–Fe–Al was higher which documents the easier incorporation of Al atoms into the bcc lattice of Fe than conversely. The mean crystallite sizes for all detected phases have changed from approximately 30 nm after 5 h of milling to 10 nm in the final powder. Nevertheless the size of grains and grain

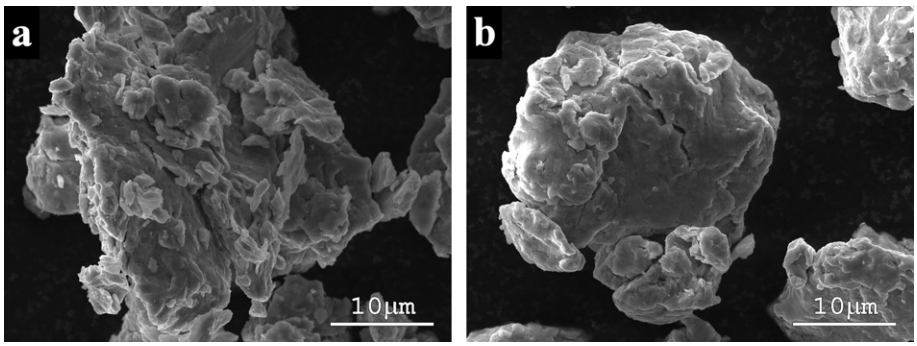

Fig. 1. SEM images of randomly selected particles of the mechanically alloyed Fe–Al after 5 (a) and 30 (b) h of milling in nitrogen atmosphere.

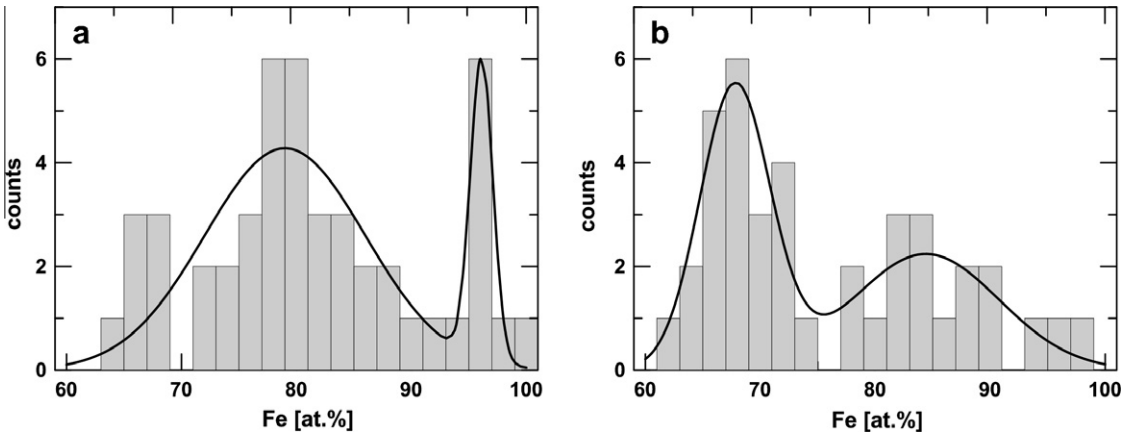

Fig. 2. Distribution curves of chemical composition (Fe content) of particles in mechanically alloyed samples MA/5 (a) and MA/30 (b).

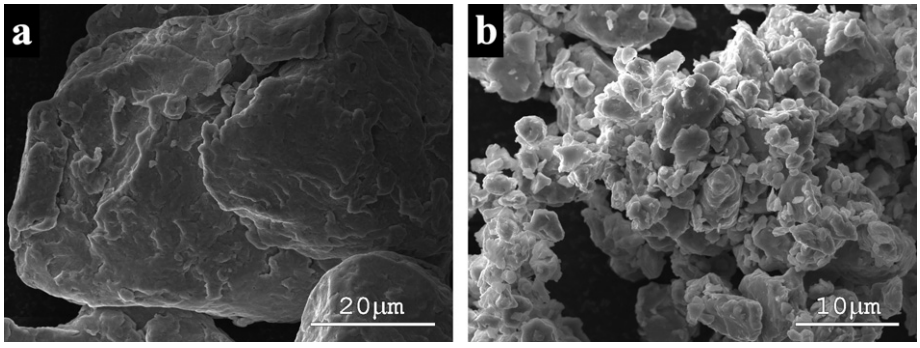

Fig. 3. SEM images of randomly selected particles of the mechanically pulverized $Fe_{82}Al_{18}$ after 10 (a) and 30 (b) h of milling in nitrogen atmosphere.

agglomerates is substantially larger. The iron nitride formation is probably connected with a large amount of Fe particles of sizes of at most a few μm (as used e.g. in the classical work by Lehrer [17]). Such particles, above all their large surface areas, can be more easily brought into equilibrium with nitrogen atmosphere involving formation either solid solutions and/or iron nitrides in accordance with the Lehrer diagram. During the milling the Fe and Al particles are fractured into smaller ones, cold welded and mutually alloyed but some of the fractured Fe particles, predominantly their defected surfaces are exposed also to the nitrogen gas. The N atoms can be trapped in defects and easily diffused into iron.

The diffraction patterns of the grinded $Fe_{82}Al_{18}$ (MM) alloy show almost symmetric lines with peak positions corresponding to an approximate composition of $Fe_{80}Al_{20}$. The line-broadening reflects a decrease in crystallite size changing from 20 nm after the first step of milling to approximately 8 nm in the final state. The slight decrease in the lattice parameter is seen in Table 1. No nitride phase was detected in the MM sample even if the alloy was also treated in nitrogen atmosphere. The reason probably consists in a "bulk-like" character of the $Fe_{82}Al_{18}$ pieces. An inwards diffusion of nitrogen is then limited similarly as the nitrogen diffusion into bulk iron. According to equilibrium Fe–N diagram [14], the solubility limit of nitrogen in iron is temperature dependent, and at 450 °C the iron-based alloy can absorb up to 5.7–6.1 at.% of N. But the temperature during milling did not exceed 100 °C. Therefore the nitrogen atoms are probably only trapped and de-trapped from the defects at the particle surfaces without a nitrogen solid solution and/or nitride formation. The paramagnetic Fe_2Al_5 phase, with hyperfine parameters similar to those of the MA samples, was detected at first by Mössbauer spectrometry

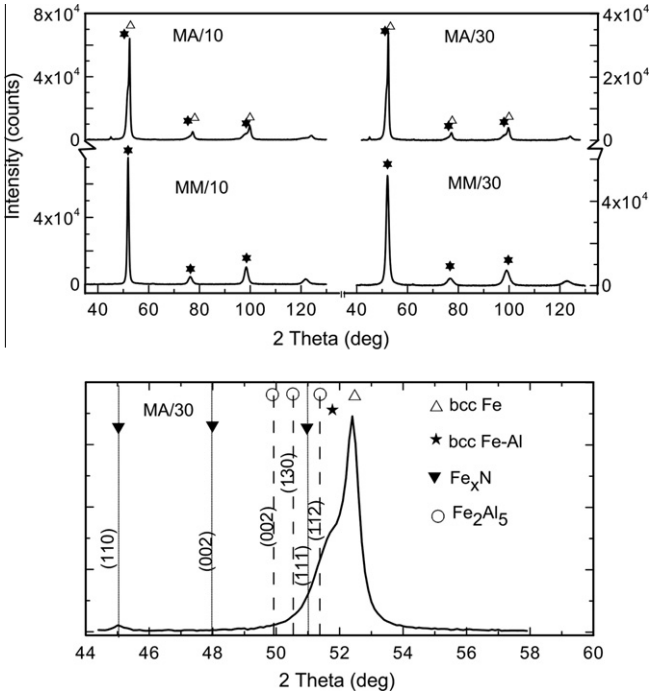

Fig. 4. X-ray diffraction patterns of mechanically alloyed (MA) and milled (MM) Fe–Al samples. The numbers denote milling time; the symbols in the upper panel reflect α-iron (Δ), and bcc Fe–Al (★). The bottom panel shows a more detailed analysis of the mechanically alloyed (MA) sample after 30 h of milling.

Table 1
The results of rietveld analysis of mechanically alloyed (MA) and milled (MM) Fe–Al; *a*, *b*, *c* -lattice parameters, *I* – phase content.

Sample	Phase	*a* (nm)	*b* (nm)	*c* (nm)	*I* (wt.%)
MA/5	α-Fe	0.2869(1)			35.5(8)
	α-$Fe_{1-x}Al_x$	0.2904(3)			41.5(6)
	ε-Fe_xN	0.4647(5)		0.4455(5)	6.5(3)
	Fe_2Al_5	0.7640(11)	0.6307(10)	0.4167(10)	16.5(6)
MA/10	α–Fe	0.2867(2)			32.9(6)
	α-$Fe_{1-x}Al_x$	0.2903(2)			38.2(4)
	ε-Fe_xN	0.4653(3)		0.4430(5)	8.5(5)
	Fe_2Al_5	0.7575(11)	0.6310(9)	0.4156(5)	20.4(3)
MA/20	α-Fe	0.2868(1)			32.1(2)
	α-$Fe_{1-x}Al_x$	0.2904(2)			41.8(3)
	ε-Fe_xN	0.4728(1)		0.4390(1)	8.5(2)
	Fe_2Al_5	0.7513(11)	0.6388(8)	0.4114(5)	17.6(6)
MA/30	α-Fe	0.2866(3)			33.8(2)
	α-$Fe_{1-x}Al_x$	0.2898(2)			39.1(4)
	ε-Fe_xN	0.4651(1)		0.4383(1)	10.0(3)
	Fe_2Al_5	0.7549(12)	0.6251(8)	0.4171(6)	17.1(1)
MM/10	α-$Fe_{80}Al_{20}$	0.2898(1)			90.0(2)
	Fe_2Al_5	0.7654(16)	0.6322(14)	0.4006(6)	10.0(3)
MM/20	α-$Fe_{80}Al_{20}$	0.2895(1)			80.7(3)
	Fe_2Al_5	0.7552(6)	0.6407(5)	0.4142(3)	19.3(7)
MM/30	α-$Fe_{80}Al_{20}$	0.2884(2)			78.6(2)
	Fe_2Al_5	0.7460(11)	0.6320(9)	0.4131(5)	21.4(5)

and retroactively, the ICSD structural data for Fe_2Al_5 were used for X-ray diffraction patterns analysis of the MM sample.

3.3. Magnetic measurements

The powders of MA/5, MA/30, MM/10, and MM/30 were pressed into small disks of about 3 mm in diameter. Such samples were used for the hysteresis and thermomagnetic (TM) measurements to follow changes in magnetic properties. The hysteresis loops were measured at room temperature before (initial) and after (final) thermomagnetic measurements and the magnetic parameters are summarized in Table 2. Relative accuracy of parameters determined from the measured curves is approximately 5%.

The initial values of coercivity are determined by a number of factors as crystallite size, stresses induced during milling similarly as defects formed at the particle surfaces, and formed phases in the case of mechanical alloying. The saturation magnetization is not sensitive to most of these factors. It does not change at MM samples in opposite to MA samples at which the contributions of the formed phases have to be taken into account. The final values obtained after TM measurements are at all samples more uniform due to annealing out of stresses and achieving the similar crystallite size. Lower values of the saturation magnetization at the MA samples can be ascribed to a mixture of observed phases: bcc–Fe–Al, ε–Fe_xN, and Fe_2Al_5. Differences between the MA and MM samples can be followed also from the TM curves depicted in Fig. 5.

The magnetization of the MA samples increases between 298 K and 575 K. A slight decrease above this temperature is connected with transformation of the ε-Fe_xN (*x* ranges between 2.6 and 2.8) from the ferromagnetic into the paramagnetic state and with following stress annealing. Around 750 K the magnetization begins to rise due to a stabilization of composition obtained and then it steeply decreases above 900 K. The Curie temperatures of 946 K and 925 K correspond to 20 at.% and 21 at.% of aluminum in the alloy, respectively [18]. The magnetization of the MM/10 sample increases smoothly with temperature up to the transformation of the Fe–Al phase into the paramagnetic state. At the MM/20 and MM/30 samples, it increases up to 673 K and then it has a plateau evidencing the annealing out of the defects and stabilizing the composition. Then it rises and above 997 K steeply decreases again due to transition of Fe–Al into the paramagnetic state. While the T_C of the MM/10 sample matches the $Fe_{82}Al_{18}$ composition, the aluminum content in the MM/20 and MM/30 is slightly below 18 at.%Al [18].

3.4. Mössbauer spectrometry

The examples of Mössbauer spectra of Fe–Al samples are depicted in Fig. 6; MA – left panel, MM – right panel. At first sight the spectra of the MA and MM samples differ substantially. The spectra of all samples were decomposed into individual six-line and double-line components representing ferromagnetic and paramagnetic phases, respectively. The spectra of MA samples after 5 (a) and 30 (b) h of milling consist of the intensive α-Fe component (dotted pattern), a sum of sub-components reflecting various position of Al atoms in the nearest and next-nearest neighborhood of resonating Fe atom (grey pattern), of a ferromagnetic ε-Fe_xN phase according to XRD results (black), and of the distribution of hyperfine inductions (dotted line) ascribed to a highly defected interfacial phase. Moreover doublets in the center of the measured spectrum represent a paramagnetic phase. The spectrum of the $Fe_{82}Al_{18}$ as prepared bulk sample measured in backscattering geometry (Fig. 6 right panel, a) represents a sum of components reflecting also various positions of Al atoms in the nearest and next-nearest neighborhood of resonating Fe atoms with the mean value of hyperfine induction of (28.4 ± 0.2) T. The milling has changed stepwise the results. Next to the components representing the bcc–Fe–Al, a broadened six-line spectrum and a double-line component in the central part were detected. The broadened spectrum represents the highly defected particle surfaces and grain boundaries while the doublet belongs to a paramagnetic phase, very probably to Fe_2Al_5 in agreement with XRD results. The very similar hyperfine parameter can be found in literature also for,

Table 2
Magnetic parameters determined from the hysteresis and thermomagnetic curves in the initial as-milled state (denoted by "1") and final after thermomagnetic measurements (denoted by "2"); coercivity H_c, remnant, J_r, and saturation, J_s, magnetization, Curie temperature T_C.

Sample	Initial			Final			
	H_{c1} (kA/m)	J_{r1} (Am^2 kg^{-1})	J_{s1} (Am^2 kg^{-1})	H_{c2} (kA/m)	J_{r2} (Am^2 kg^{-1})	J_{s2} (Am^2 kg^{-1})	T_C (K)
MA/5	7.1	8.6	156.9	2.0	2.9	152.9	946
MA/30	7.5	8.9	162.6	1.4	2.5	150.6	925
MM/10	2.4	2.1	175.1	1.4	1.1	171.9	970
MM/30	2.7	2.5	174.2	2.4	2.3	174.2	1019

Relative accuracy of parameters determined from the measured curves is approximately 5%.

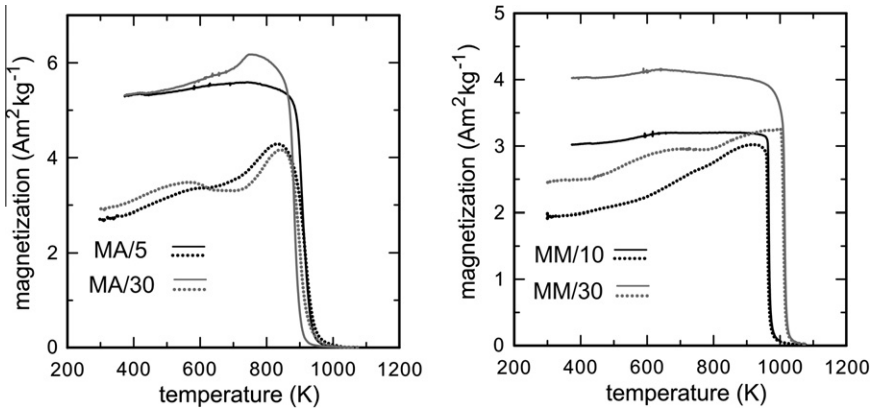

Fig. 5. Thermomagnetic curves at the increasing (dotted lines) and decreasing (full lines) temperatures of mechanically alloyed (MA for 5 and 30 h of milling) and ball milled (MM for 10 and 30 h of milling) Fe–Al samples.

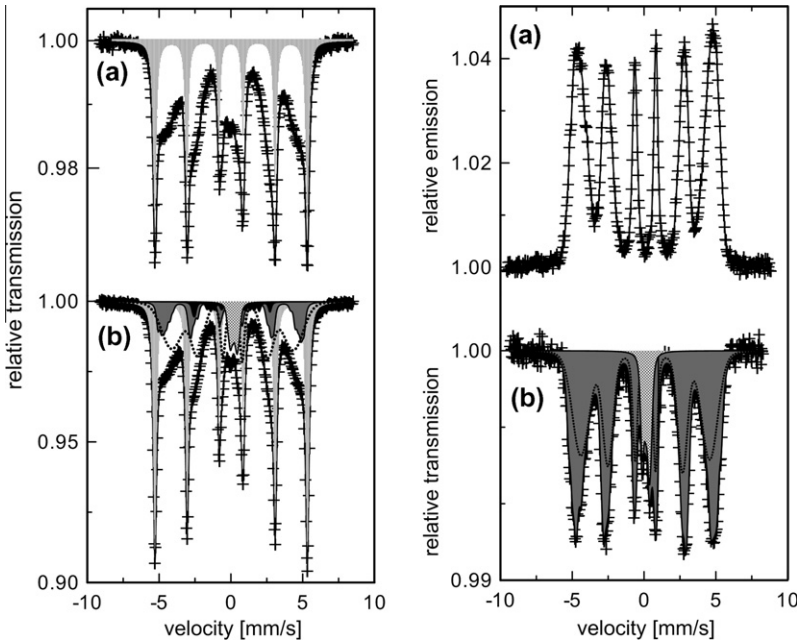

Fig. 6. Mössbauer spectra of Fe–Al samples: MA (left panel; a-5 h, b-30 h of milling) and of MM (right panel; a-backscattered spectrum of initial bulk $Fe_{82}Al_{18}$ alloy, b-transmission spectrum after 30 h of milling).

e.g., $FeAl_3$ phase [19] or $FeAl_2$ phase [20,21]. Nevertheless, the present XRD measurements facilitate the Fe_2Al_5 phase. The final spectrum of the powdered $Fe_{82}Al_{18}$ sample (MM/30) is depicted in Fig. 6b in the right panel. The mean hyperfine induction of the bcc–Fe–Al phase of 30.2 T reflects a decrease in Al content in comparison to initial composition. The hyperfine parameters for the MA and MM samples after 30 h of milling and for all detected phases are summarized in Table 3.

The room temperature spectrum in Fig. 7 represents the state of the MA/30 sample after the TM measurement. It documents the formation of a more uniform alloy composed of 84% of bcc Fe–Al the spectrum of which is represented by 5 sub-spectra (grey) with

Table 3
Hyperfine parameters for MA and MM Fe–Al samples after 30 h of milling; B – hyperfine induction, ΔB – width of distribution of hyperfine induction, δ – isomer shift, Δ – quadrupole splitting, A – relative area.

Phase	MA					MM				
	B (T)	ΔB (T)	δ (mm/s)	Δ (mm/s)	A (%)	B (T)	ΔB (T)	δ (mm/s)	Δ (mm/s)	A (%)
α-Fe	33.0(1)	–	0.018(1)	0.000(1)	50.7(5)					
bcc–FeAl	29.4(1)		0.052(2)	0.015(1)	10.6(2)	30.2(2)		0.080(2)	0.002(1)	84.3(2)
ε-Fe_xN	18.6(1)	–	0.169(13)	–	4.6(5)					
Fe_2Al_5			0.210(13)	0.460(12)	4.3(3)			0.184(22)	0.460(27)	2.0(3)
Defect	26.3(1)	9.6(2)	0.114(4)	0.012(1)	29.8(9)	26.1(1)	18.2(2)	0.180(18)	0.068(20)	13.7(2)

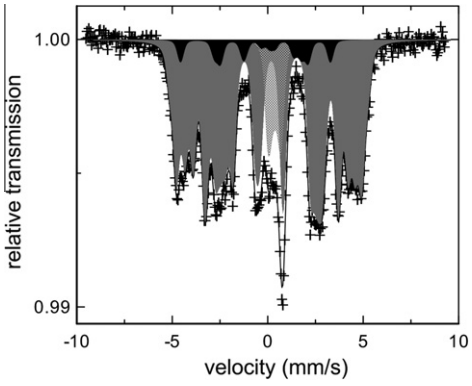

Fig. 7. Mössbauer spectrum of mechanically alloyed sample (MA/30) measured at room temperature after thermomagnetic curve measurement.

the mean hyperfine induction of 26.1 T. The next 6% stands for iron nitride (black) of the mean hyperfine induction of 19.4 T which coincides with that of ε-$Fe_{2.6}N$ [22]. The last 10% belongs to paramagnetic Fe_2Al_5 (criss-cross) of the same hyperfine parameters as presented by Yelsukov et al. [16]. The component represented by the distribution of hyperfine magnetic induction and ascribed to the highly defected interfacial phase was annealed out according to the TM results. Similar spectrum was obtained also for the MM/30 sample after the thermomagnetic cycle.

4. Conclusions

The systematic investigations document an influence of the oversaturated nitrogen atmosphere and the severe mechanical deformation in the process of ball milling on the mixture of the Fe and Al powders and on the $Fe_{82}Al_{18}$ bulk alloy in a form of small pieces. It is shown that the bcc–Fe–Al alloy is formed from individual elements after 5 h of milling in agreement with findings of other authors. However, the treatment in nitrogen atmosphere contributes also to a formation of a nitride phase. Its formation was observed at the mechanically alloyed sample only because of much easier nitrogen diffusion into the iron particles enhanced by their large surfaces and defect structure formed during milling. The ferromagnetic ε-Fe_xN was established by X-ray diffraction and Mössbauer phase analysis and confirmed by thermomagnetic measurement. The pieces of $Fe_{82}Al_{18}$ have embodied substantially smaller surface areas and represent a rather bulk-like alloy than a powder. Therefore a diffusion of nitrogen is more difficult. Nevertheless they are also exposed to severe deformation contributing to grain refinement and defect formation facilitating the changes in the chemical composition at surfaces of rising particles. Only this can explain the formation of a small amount of the paramagnetic Fe_2Al_5 phase. The magnetic measurements done at both samples after 5 and 30 h of milling yielded a higher coercivity and a lower saturation magnetization at mechanically alloyed samples due to a presence of the magnetically harder nitride phase. Owing to the elevated temperature during the thermomagnetic curve measurements, the coercivities of both samples have aligned, the grain size has decreased, and defect rich regions were annealed out as it followed from X-ray diffraction, thermomagnetic and Mössbauer measurements, respectively. The lower saturation magnetization of the mechanically alloyed sample influenced by 16% of nitride phases was stable against the elevated temperature.

Acknowledgements

The authors thank Dr. I. Turek for his valuable comments, Dr. M. Hapla for magnetic measurements (both IPM, AS CR Brno), Dr. D. Janickovic (IP SAS Bratislava, Slovakia) for preparation of the $Fe_{82}Al_{18}$ ingot, and the Czech Science Foundation (P108/11/1350) for financial support.

References

[1] J.L. Jordan, S.C. Deevi, Intermetallics 11 (2003) 507.
[2] R.S. Sundar, S.C. Deevi, Mat. Sci. Eng. A357 (2003) 124.
[3] G. Hasemann, J.H. Schneibel, E.P. Georgie, Intermetallics 21 (2012) 56.
[4] O. Kubachewski, In: Iron Binary Phase Diagrams, Springer, Berlin, 1986.
[5] H. Gengnagel, M.J. Besnus, H. Danan, Phys. Stat. Sol. A13 (1972) 499.
[6] R.A. Varin, T. Czujko, J. Bystrzycki, A. Calka, Mat. Sci. Eng. A329 (2002) 213.
[7] E.P. Yelsukov, E.V. Voronina, V.A. Barinov, J. Magn. Magn. Mat. 115 (1992) 271.
[8] C. Suryanarayana, Prog. Mater. Sci. 46 (2001) 1.
[9] E. Jartych, J. Zurawicz, D. Oleszak, M. Pekala, J. Sarzynski, M. Budzynski, J. Magn. Magn. Mat. 186 (1998) 299.
[10] R.A. Young (Ed.), in: The Rietveld method International union of crystallography book series, Oxford University Press; 1993.
[11] T. Zak, Y. Jiraskova, Surf. Interf. Anal. 38 (2006) 710.
[12] Z. Hamleti, A. Guittoum, S. Bergheul, N. Souami, K. Taibi, M. Azzaz, Advances in Key Eng. Mat. Book Series, Adv. Mat. Res. 214 (2011) 490.
[13] L.E. Zamora, G.A. Perez Alcazar, G.Y. Velez, J.D. Betancur, J.F. Marco, J.J. Romero, A. Martinez, F.J. Palomares, J.M. Gonzales, Phys. Rev. B 79 (2009) 094418.
[14] H.A. Wriedt, N.A. Gokcen, R.H. Nafziger, Bull. Alloys Phase Diagr. 8 (1987) 355.
[15] F. Cardellini, V. Contini, R. Gupta, G. Mazzone, A. Montone, A. Perin, G. Principi, J. Mater. Sci. 33 (1998) 2519.
[16] E.P. Yelsukov, A.L. Ulyanov, A.V. Protasov, D.A. Kolodkin, Phys. Met. Metall. 113 (2012) 602.
[17] E. Lehrer, Zeitschrift Elektrochemie. Angewandte phys, Chemie 36 (1930) 383.
[18] W. Köster, T. Gödecke, Z. Metallkunde 71 (1980) 765.
[19] E. Jartych, J.K. Zurawicz, D. Oleszak, J. Sarzynski, M. Budzynski, Hyperfine Interactions 99 (1996) 389.
[20] D. Maltas, E. Svab, Z. Somogyvari, G. Andre, L.F. Kiss, J. Balogh, L. Bujdoso, T. Kemeny, I. Vincze, Phys. Rev. B 73 (2006) 012401.
[21] Ji Chi, Yang Li, F.G. Vagizov, V. Goruganti, J.H. Ross, Phys. Rev. B 71 (2005) 024431.
[22] M. Kopcewicz, A. Jagielski, A. Turos, D.L. Williamson, J. Appl. Phys. 71 (1992) 4217.